Article

Recognition of the Interaction Mechanisms between Water and Land Resources Based on an Improved Distributed Hydrological Model

Jianwei Wang [1], **Xizhi Lv** [1], **Tianling Qin** [2,*], **Yongxin Ni** [1,3], **Li Ma** [1], **Qiufen Zhang** [1], **Hanjiang Nie** [4,5], **Zhenyu Lv** [6], **Chenhao Li** [7,8], **Xin Zhang** [2] **and Jianming Feng** [9]

[1] Yellow River Institute of Hydraulic Research, Henan Key Laboratory of Yellow Basin Ecological Protection and Restoration, Zhengzhou 450003, China

[2] State Key Laboratory of Simulation and Regulation of Water Cycle in River Basin, China Institute of Water Resources and Hydropower Research, Beijing 100038, China

[3] College of Hydrology and Water Recourses, Hohai University, Nanjing 210098, China

[4] Key Laboratory for Geographical Process Analysis & Simulation of Hubei Province, Wuhan 430079, China

[5] School of Urban and Environmental Sciences, Central China Normal University, Wuhan 430079, China

[6] China Three Gorges Corporation, Wuhan 430010, China

[7] Beijing Laboratory of Water Resources Security, Capital Normal University, Beijing 100048, China

[8] Beijing Institute of Hydrogeology, College of Resource Environment and Tourism, Capital Normal University, Beijing 100048, China

[9] School of Water Conservancy and Civil Engineering, Zhengzhou University, Zhengzhou 450001, China

* Correspondence: qintl@iwhr.com

Abstract: Conflicts between humans and land use in the process of using water and conflicts between humans and water resources in the process of using land have led to an imbalance between natural ecosystems and socio-economic systems. It is difficult to understand the impact of the processes of water production and consumption on land patches and their ecological effects. A grid-type, basin-distributed hydrological model was established in this study, which was based on land-use units and coupled with groundwater modules to simulate the water production and consumption processes in different units. By combining land use and net primary productivity, the runoff coefficient and the water use efficiency (NPP/ET) of different land units were used as indicators to characterize the interaction between water and land resources. The results showed that the average runoff coefficients of cultivated land, forest land and grassland were 0.7, 0.5 and 0.9, respectively. Moreover, the average runoff coefficients of hills, plains and basins were 0.7, 0.7 and 0.8, respectively. The NPP produced by the average unit, evapotranspiration, in cultivated land, forest land and grassland was 7 (gC/(m^2•a))/mm, 0.7 (gC/(m^2•a))/mm and 0.2 (gC/(m^2•a))/mm, respectively. These results provide quantitative scientific and technological support in favor of the comprehensive ecological management of river basins.

Keywords: distributed hydrological model; water and land resources; evapotranspiration; runoff coefficient; Sihe River Basin

1. Introduction

Water and land resources are essential for humanity's survival and development. With the continuous acceleration of urbanization, the urban population is growing rapidly, the scale of infrastructure construction is increasing, and the human demand for water and land resources is gradually increasing [1,2]. Because of the limited supply of water and land resources, the imbalance between water and land use among departments and industries has become increasingly prominent. The failure to coordinate our use of water and land resources has led to a series of natural disasters, which have affected human development and the ecosystem's health [3,4]. Extreme rainfall and prolonged droughts can affect plant

growth, which affects soil water content, which, in turn, affects soil biomass [5,6]. Therefore, identifying the relationship between water and land resources is of great significance in improving the utilization efficiency of water and land resources and in alleviating the conflict between social development and water and land resources.

Scholars have conducted research into the interaction between water and land resources through field experiments, laboratory experiments, remote sensing interpretation and hydrological model simulations. From the perspective of hydrological models, the most commonly used hydrological models include the SWAT model [7], which can be used in the cost-effective management of water resources in river basins, and CLM [8], which is a land surface process that can be used to assess the impact of land on vegetation. However, these models are insufficient in the simulation of groundwater processes. Further models include HYDRUS [9], which produces better simulations of soil movement processes, and MODFLOW [10], which is good at simulating underground movement processes. However, these models are not able to simulate surface water processes. VIC [11] is a large-scale, semi-distributed hydrological model, which can be used for drought assessments; however, it focuses on vertical simulation and lacks horizontal simulation. MIKE [12] produces a better simulation of river flow processes and can be used to assess the inundation effects of floods on river channels; however, its simulations of slope hydrological processes are insufficient. WEP [13] is used for watershed hydrological simulations and can be used to study the impact of land-use changes on the water cycle process; however, its simulation of soil water and groundwater processes need to be improved. Of course, there are many other hydrological models. The aforementioned models are representative of the types of models available. Each model has its own advantages, but regarding the simulation of the whole process of the water cycle in river basins, they are all insufficient in the simulation of one or more hydrological processes.

Therefore, in view of the above research status, in this study, we drew on the advantages of various numerical models and established a new watershed-distributed hydrological model based on a land-use type grid. The interaction laws of the water and land resources in each land unit were analyzed, which have provided technical support in favor of the rational allocation of water and soil resources and the comprehensive management of river basins. The main research contents of this paper are as follows: (1) the Python language was used to compile the new hydrological model; (2) the law of interaction between water and soil resources was observed and studied using this model.

2. Materials and Methods

Runoff is a direct manifestation of water resources, and net primary productivity is a direct manifestation of land productivity. Therefore, the runoff coefficient was selected to reflect the impact of land resources on water resources, and the ratio of evapotranspiration to NPP (net primary productivity) was selected to reflect the impact of water resources on land resources so that we could study the interaction mechanisms between water and land resources. The technical route is shown in Figure 1.

2.1. Study Area

The Sihe River is a first-order tributary of the Huaihe River, which is located in the north–south transitional zone of China, with a watershed area of 2613.73 km^2. The Sihe River starts from the west foot of Taipingding, Tai'an city, Shandong Province, in the north, and, finally, flows into Nanyang Lake. The watershed is high in the east and low in the west, with an average elevation of 136.9 m. The location and topography of the Sihe River Basin are shown in Figure 2.
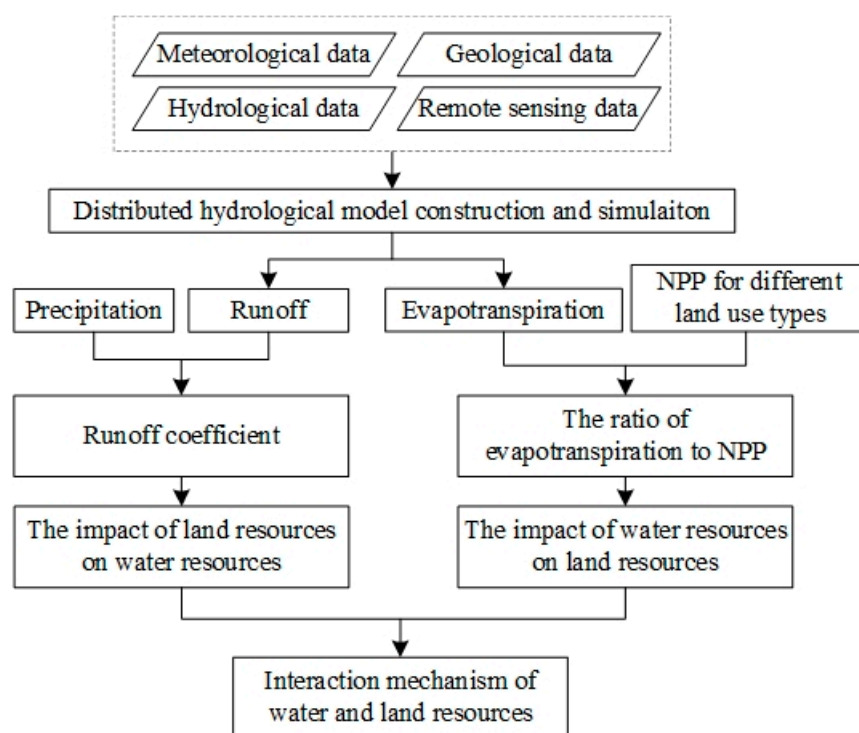
Figure 1. Schematic diagram of the research process.
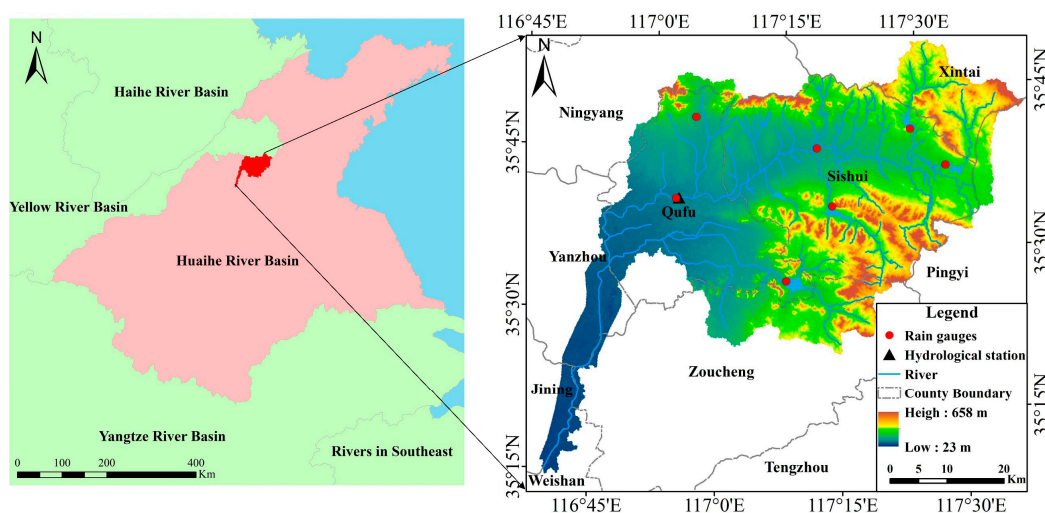
Figure 2. Location map of the study area.

The Sihe River Basin is located in a semi-humid, warm, temperate climate zone, with four distinct seasons and significant climate change. The annual average temperature in the river basin is 13~14 °C, and the number of annual average sunshine hours is 2180. According to statistics from meteorological stations, the annual precipitation in the Sihe River Basin in 2015 was 602.87 mm. The main land-use type in the Sihe River Basin is cultivated land, with an area of 1726.3 km^2, accounting for 66.05% of the river basin. Residential/industrial land and grassland have areas of 384.8 km^2 and 275.7 km^2, respectively, accounting for 14.72% and 10.55%, respectively. The total area covered by forest, water and unused land accounts for 8.68%. Forest and grassland areas are mainly distributed in the northern and southern mountainous regions of the river basin, and the rest is cultivated land. The details are shown in Figure 3. The national land use classification standards are shown in Table 1.
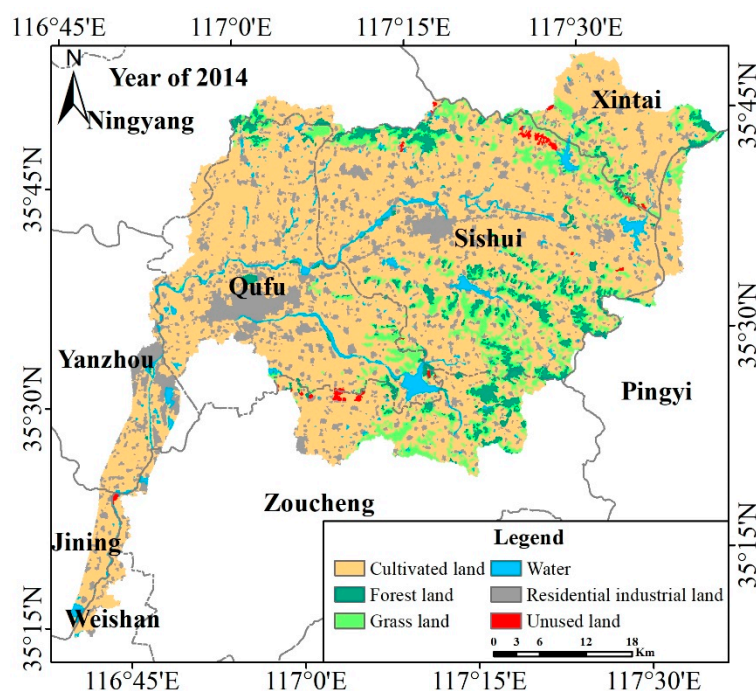
Figure 3. Current distribution of land use in Sihe River Basin.

Table 1. National land use classification standard.

Land Use Type	Contents
Cultivated land	Refers to land for planting crops, including mature cultivated land, newly reclaimed wasteland, leisure land, rotation land and grassland rotation land; agricultural fruit, mulberry and agricultural and forestry land mainly used for planting crops; tidal land and tidal flats that have been cultivated for more than three years.
Forest land	Refers to growing trees, shrubs, bamboos, coastal mangroves and other forestry land.
Grassland	Refers to all kinds of grasslands with a coverage of more than 5% mainly composed of growing herbs, including shrub grasslands dominated by grazing and sparse forest grasslands with a canopy closure of less than 10%.
Water	Refers to natural land waters and land for water conservancy facilities.
Residential industrial land	Refers to urban and rural settlements and industrial, mining and transportation land other than counties and towns.
Unused land	Refers to land that has not been used at present, including land that is difficult to use.

2.2. Model Construction

The model was based on the actual spatial distribution of land units to form a refined simulation unit, with independent land-use types. It coupled the distributed hydrological model of the watershed with the groundwater model to build a new watershed model, and it was written in Python. The structure and diagram of the model are shown in Figure 4. The land in the grid was divided according to the current national land use classification system. Each grid unit had an independent land-use type, and the corresponding water cycle process was simulated for the different land-use types. For cultivated land, forest land and grassland, it needed to consider elements such as vegetation interception, depression retention, soil thickness, vegetation transpiration and soil evaporation. The three land types considered the same elements as in the water cycle simulation; however, the parameters involved in the simulated hydrological elements were different due to different factors as follows: different land types have different values; water areas and residential construction sites directly generate runoff; and unused land is treated as bare land. If the amount of water infiltrated into the soil exceeds the field capacity, the excess water will recharge the

groundwater. This model coupled surface and groundwater process simulations, simulated the hydrological process of each grid and provided technical support for the analysis of spatial hydrological laws.
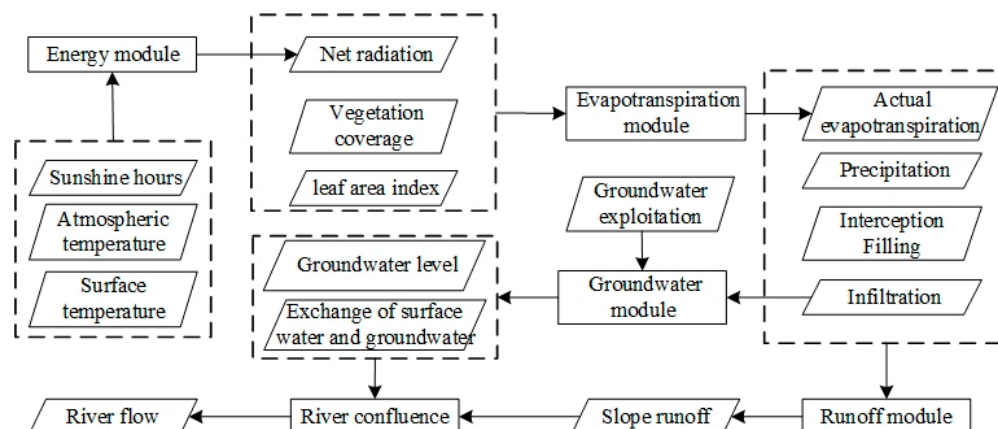

Figure 4. Technical diagram for building the model.

2.2.1. Model Structure

The model consisted of a vertical and horizontal structure.

The land-use types in the grid were assigned according to the current national land-use classification system. Each grid unit had an independent land-use type, and the corresponding water cycle process simulation was adopted for the different land-use types. It produced a hydrological cycle simulation of cultivated land, forest and grassland, as the underlying surface needed to consider factors such as vegetation interception, depression storage, soil thickness, vegetation transpiration and soil evaporation. The cultivated land, forest land and grassland considered the same elements as in the water cycle simulation, but the parameters involved in the simulated water cycle elements had different values depending on the land type. Water areas and residential industrial land directly generate runoff, and unused land is regarded as bare land. If the amount of water infiltrated into the soil exceeds the filed capacity, the excess water will recharge the groundwater. A schematic diagram of the water cycle is shown in Figure 5.
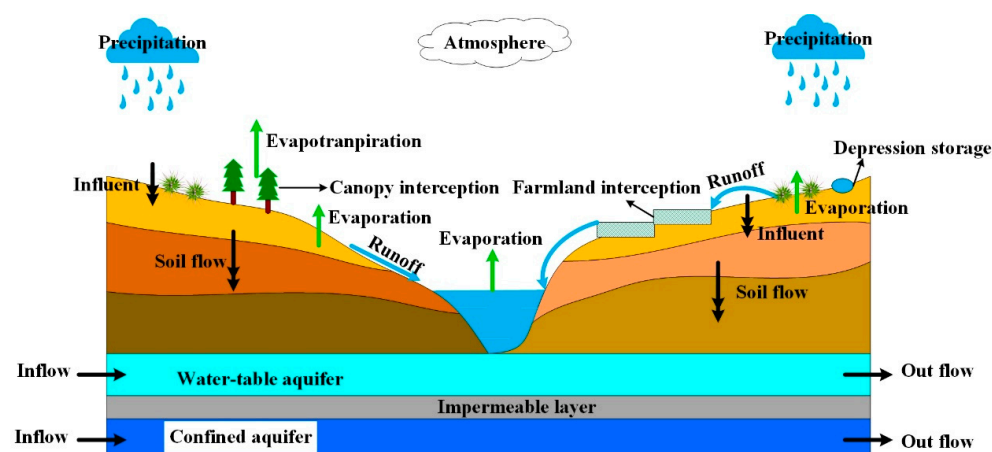
Figure 5. Schematic diagram of the water cycle.

The horizontal process included three aspects: slope confluence, river confluence and groundwater flow. The runoff of each grid was obtained through the vertical process, and then the confluence calculation was performed based on the grid flow direction. The calculation sequence was from upstream to downstream, and from slope to river. The horizontal structure of the model is shown in Figure 6.
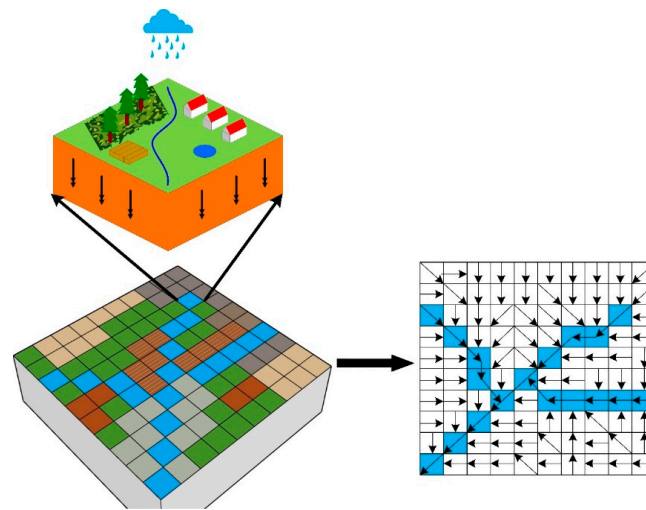
Figure 6. Horizontal structure of the model.

2.2.2. Simulation Elements and Equations

The model's simulation process included six main aspects in accordance with the water cycle process: evapotranspiration, infiltration, runoff, soil flow, groundwater and confluence. The calculation formula and key parameters of the simulation process are shown in Table 2.

Table 2. Hydrological model's simulation elements, calculation formulas and key parameters.

Elements	Content	Formula	Key Parameter
Evapotranspiration	Vegetation transpiration	Penman–Monteith [13]	Plant community resistance, root layer thickness and aerodynamic resistance.
	Vegetation interception evaporation	Penman [14]	Vegetation coverage, leaf area index and maximum vegetation interception.
	Water evaporation	Penman	Aerodynamic impedance and net radiation.
	Bare soil evaporation	Revised Penman [15]	Field capacity and evaporation efficiency coefficient.
	Urban surface evaporation	Penman	Maximum depression storage capacity, depression storage capacity and area ratio of urban buildings in impervious areas.
Infiltration	Vertical infiltration	Green–Ampt [16]	Infiltration capacity, hydraulic conductivity, saturated water content, soil layer thickness and capillary suction.
Runoff	Infiltration excess runoff yield	Horton slope runoff	Maximum depression depth and soil infiltration capacity.
	Saturation excess runoff yield	Saturated slope runoff	Maximum depression storage depth, soil infiltration capacity, soil hydraulic conductivity, vegetation coverage, soil layer thickness and saturated soil moisture content.
Soil runoff	Soil water movement	Product of the hydraulic conductivity	Soil hydraulic conductivity and thickness of unsaturated soil layer.
Groundwater	Groundwater movement	Darcy formula	Groundwater level, storage coefficient, hydraulic conductivity, high aquifer bottom and aquifer thickness.
Confluence	Slope/river confluence	Motion wave equation	Manning coefficient, hydraulic radius, unit ground surface or river slope and length of river channel.

(1)   Confluence raster calculation

Both the slope confluence and river confluence were calculated using the kinematic wave model. Based on the river network system generated by DEM, the topological relationship and calculation sequence of the slope grid and river grid were determined by confluence and were calculated first. Next, the river confluence was calculated. The water balance (Equation (2)) in the grid was constructed using Equation (1)—the continuity equation. We substituted the Manning formula (Equation (3)) and the river section (Equation (4)) into the water balance equation to digitize the motion wave equation. In this study, the river channel was generalized into a rectangular channel, and the slope confluence was generalized into a wide and shallow channel. The water balance in the grid is shown in Figure 7.
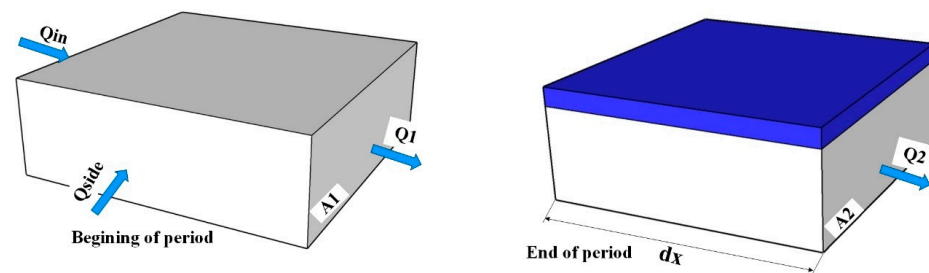
Figure 7. Schematic diagram of water balance in the grid.

Continuity equation:

$$\frac{\partial A}{\partial t} + \frac{\partial Q}{\partial x} = q_L \tag{1}$$

Water balance equation:

$$(Qin - \frac{Q1 + Q2}{2}) \times \Delta t = (A2 - A1) \times dx \tag{2}$$

The Manning formula:

$$Q = \frac{A}{n} R^{2/3} S_0^{1/2} \tag{3}$$

River section equation:

$$A = b \times h \tag{4}$$

Here, $A1$ and $A2$ are the cross-sectional areas of the grid at the beginning and end of the period, respectively; Qin is the upstream inflow of the grid; $Qside$ is the lateral inflow; $Q1$ and $Q2$ are the grid outflows at the beginning and the end of the period, respectively; n is the Manning roughness coefficient; R is the hydraulic radius; S_0 is the slope gradient; b is the width of the river channel; and h is the water depth.

(2)   Refined simulation

Traditional hydrological simulation units are dominated by contour zones or large-scale grids. The proportion of the land-use area is often used as a representation of the change in the underlying surface conditions in the unit. This research was based on the actual spatial distribution of land units to form a refined simulation unit with independent land-use attributes. For the convenience of model preparation and precise simulation, we compiled the model based on the country's current land-use classification method. Different land-use types corresponded to different hydrological parameters and hydrological processes. Each simulation unit had a set of independent hydrological parameters and an independent vertical hydrological cycle simulation process. In this way, we calculated the hydrological process of each simulation unit and then conducted further research.

(3)   Coupled simulation of surface and underground water processes

This paper adopted the groundwater simulation method used in the MODFLOW model [17], which produces a better groundwater simulation. Based on Darcy's formula, the groundwater layer was subjected to three-dimensional finite difference, and the basic equation was as Equation (5). In the model, the spatial resolution of the surface and subsurface was kept the same (90 m × 90 m). In the time resolution, the simulation scale of the surface was days, and the simulation scale of groundwater was months due to the slow movement of groundwater. When all the grid daily scale simulations were completed, a variable was used to accumulate the groundwater recharge, and the groundwater was simulated once at the end of each month, and the variable was reset to zero at the same time. In the calculation of soil water, it was judged whether the soil was saturated by setting the soil saturation moisture content. Soil water content is closely related to runoff. During the rainfall process, the soil may be saturated. At this time, part of the water is surface runoff, and the other part is recharged to the groundwater at the rate of the saturated infiltration rate.

$$\frac{\partial}{\partial x}(K_{xx}\frac{\partial h}{\partial x}) + \frac{\partial}{\partial y}(K_{yy}\frac{\partial h}{\partial y}) + \frac{\partial}{\partial z}(K_{zz}\frac{\partial h}{\partial z}) - W = Ss\frac{\partial h}{\partial t} \tag{5}$$

where K is the permeability coefficient in each direction; h is the groundwater level; W is the amount of water flowing into or out of the grid; Ss is the unit water release coefficient; and $\partial h/\partial t$ is the change rate of the groundwater level over time; x, y, z represents the three-dimensional direction.

The connection between the surface and the groundwater was mainly reflected in the variable W. W contained incoming water from six directions (front, back, up, down, left and right), including infiltration recharge, water extraction from mining, evaporation consumption, etc. In the simulation process, the groundwater level changed in real time due to the change in W, which realized the coupling between the surface and the underground water.

2.2.3. Data Input and Preparation

Four types of data were used in this model: topography, meteorology and hydrology, and underlying surface and river channels. The data details are shown in Table 3.

Table 3. List of data required for the model.

Category	Data	Year	Data Resource
Topographic	DEM	/	http://www.gscloud.cn
Meteorological	Precipitation Temperature Wind speed Sunshine time Relative humidity	1953–2015	http://www.nmic.cn
Hydrological	Hydrological station runoff	1953–2015	Hydrology Department
Groundwater	Groundwater level	2005–2015	

The topographic data were based on DEM, ArcGIS was used for the hydrological analysis, and the results were converted into ASCII files for the model input. The meteorological data included daily precipitation, temperature, wind speed, sunshine time and relative temperature. The hydrological data comprised the monthly runoff data from hydrological observatories. The groundwater level data were taken from groundwater observation wells. The river channel data included the length, width and depth. The parameters involved in the model were soil pre-water content, depression storage, vegetation coverage, leaf area index, aquifer water storage rate, etc. The relevant parameters were distributed across the space through the existing data and soil vegetation characteristics and then converted into

ASCII files, which were used as the input files of the model to realize the distribution of the parameters. The input file formats in the model were text files and ASCII files. The tools used to prepare the data were ArcGIS, MATLAB, etc.

This paper collected daily data from over 53 years—between 1963 and 2015—across five weather stations and seven rainfall stations in the Sihe River Basin and surrounding areas. The Thiessen polygon of the weather stations and the rainfall stations were calculated by ArcGIS and converted into ASCII files, which were used as the model input files. The Thiessen polygon of the weather stations and rainfall stations is shown in Figure 8.
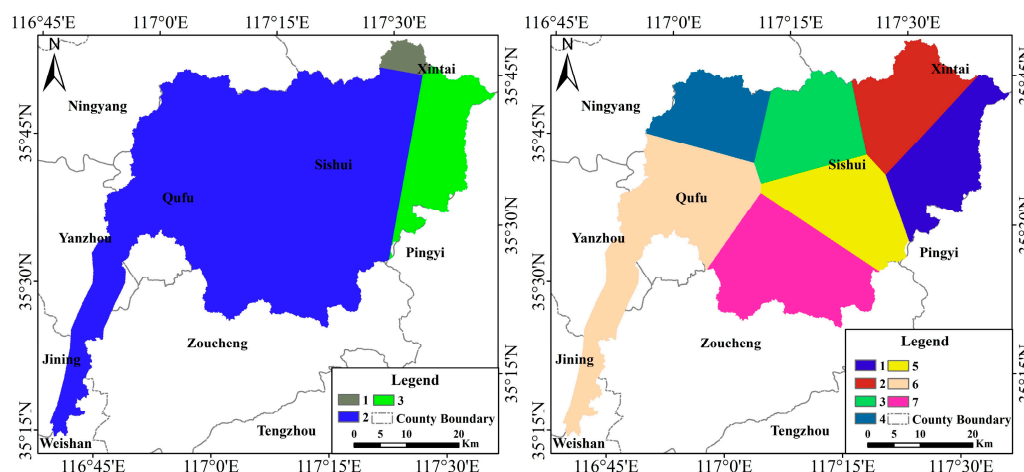
Figure 8. Thiessen polygon (**left**) weather stations; (**right**) rainfall stations.

According to the requirements of model verification, combined with the information available, the Shuyuan Hydrological Station was selected to calibrate and verify the model. The data sequence was taken from the years between 1958 and 2015. The location of the hydrological station, its catchment area and the location of the groundwater observation wells are shown in Figure 9.
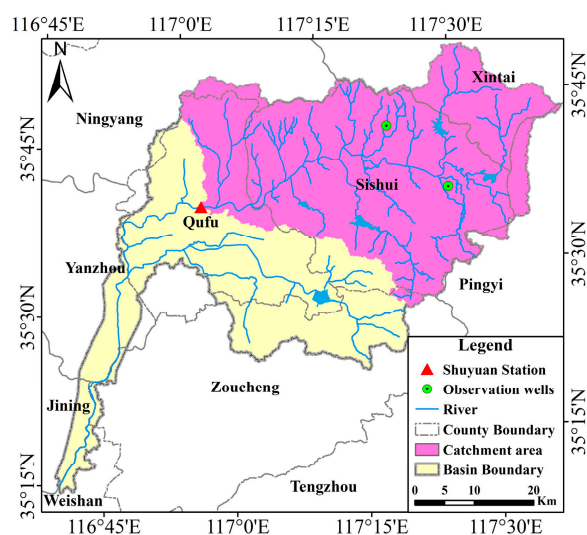
Figure 9. The location of Shuyuan Hydrological Station and groundwater observation wells.

The underlying surface data included land-use data and soil type data. According to the land-use database (1:100,000), the four phases of the land-use data in the Sihe River Basin in 1985, 1995, 2005 and 2014 were extracted, as shown in Figure 10. In the model simulation, the land-use data were used in stages (the land-use data from 1985 were used for the simulation before 1990; the land-use data from 1990 were used for the simulation

from 1990 to 2000; the land-use data from 2005 were used for the simulation from 2000 to 2010; and the land-use data from 2014 were used for the simulation after 2010).
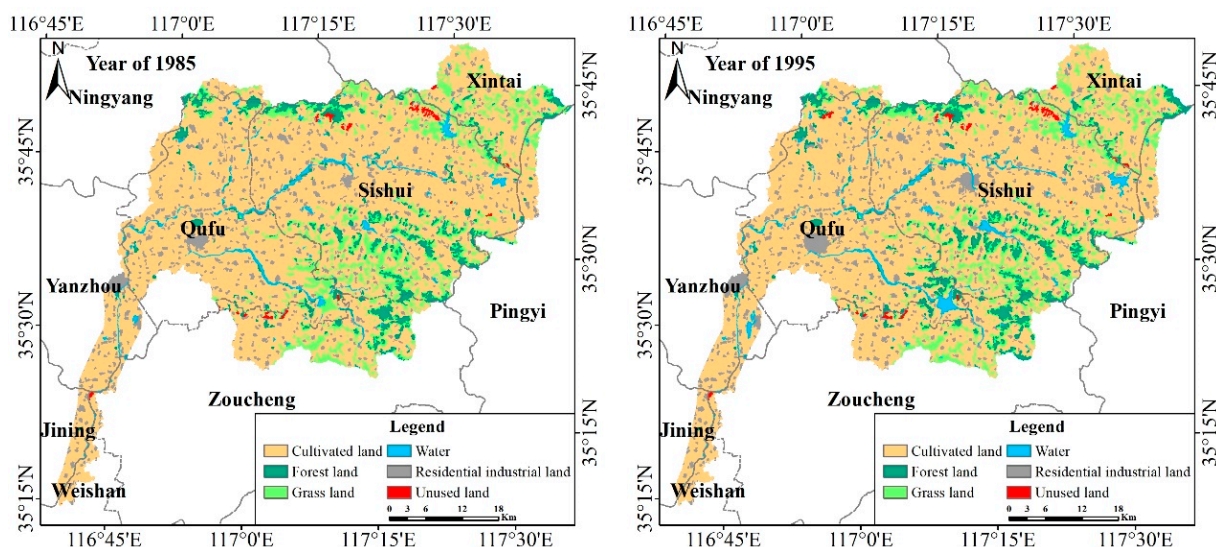
Figure 10. Land use in the Sihe River Basin during different time periods.

We extracted the soil types in the Sihe River Basin range from the national soil type database (1:100,000). The soil types were divided into four categories in the model, so the soil type data were reclassed, forming the soil type required for the model simulation. By reviewing the Chinese soil database (http://vdb3.soil.csdb.cn/), we found the soil classification belonging to the soil, which was in agreement with the other soil types in the model. This newly classified soil type was converted to an ASCII file. The soil types in the river basin are shown in Figure 11. The soil-related parameters included the following: porosity, wilting coefficient, field moisture capacity, saturated water capacity, etc. These parameters were used to determine the soil's empirical value based on the soil type.
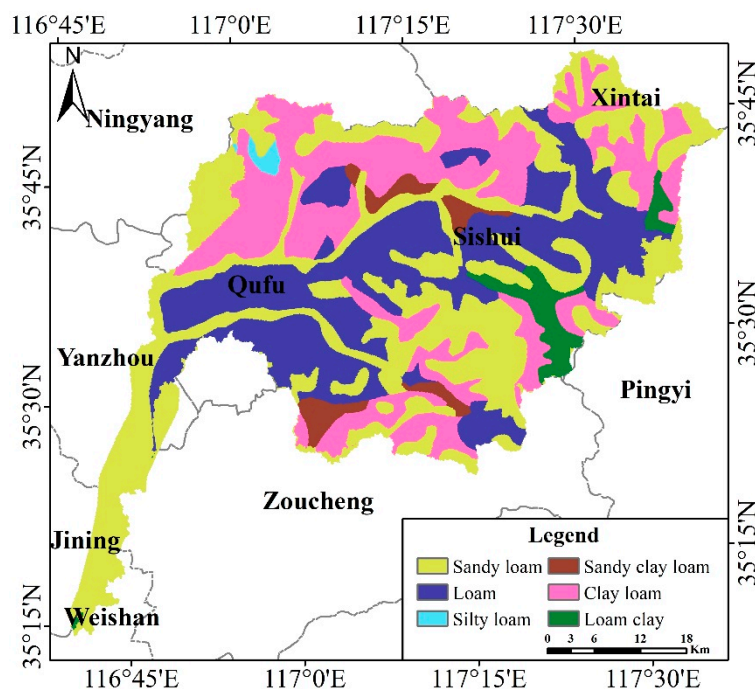
Figure 11. Soil type in the Sihe River Basin.

2.2.4. Model Usage

The prepared data were unified into the input folder. The start and end dates of the model simulation were set. Some of the parameters in the model were commonly used parameters, but others were specific to the study area. The default parameters in the model were replaced by the parameters that were specific to the study area, but the default parameters were used for those not collected. The spatial resolution of the surface and subsurface was kept the same (90 m × 90 m). In the time resolution, the simulation scale of the surface was days, and the simulation scale of groundwater was months due to the slow movement of groundwater. The model's running process is shown in Figure 12.

Figure 12. Schematic diagram of the model's running process.

2.3. Recognition Method for the Interaction Mechanisms between Water and Land Resources

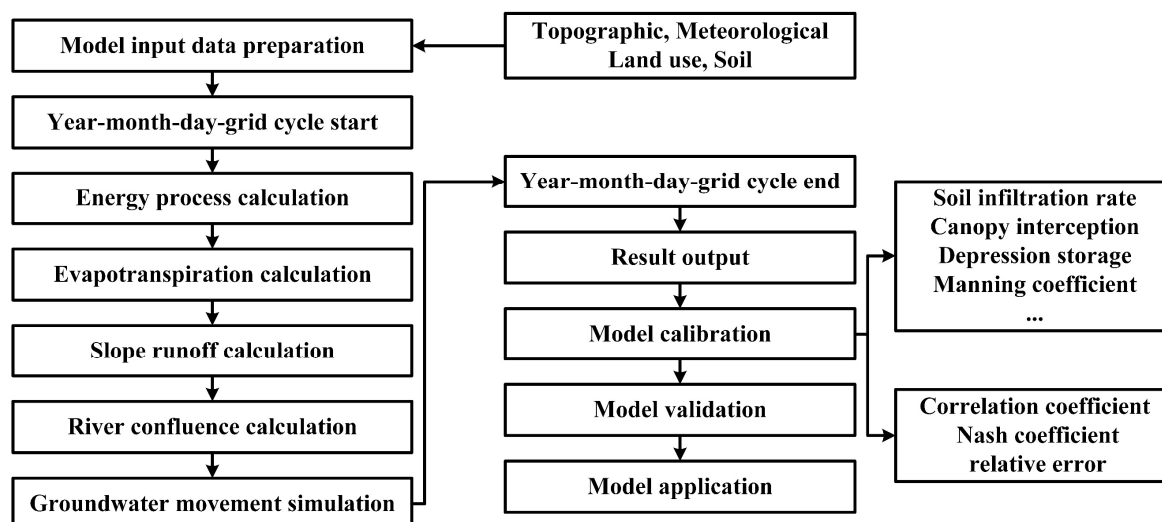Since the 20th century, water resources and land resources have undergone profound changes due to the combined effects of "natural and artificial" processes. The continuous warming of the global climate, population growth, economic development, and the increasing demand for water and land resources by humans have led to an increase in the conflict between the supply and demand of water and land resources [1,18]. Therefore, studying the interaction mechanisms between water and land resources plays an important role in alleviating the conflict between the supply and demand of water and land resources.

In this study, the hydrological model compiled by the authors was used as a tool to simulate the water cycle processes in each grid and to study their interactions with the soil and land resources. Different underlying surface conditions had different effects on the runoff generation. The runoff coefficient in each grid unit was used to study the effects of land resources on water resources, and the NPP per unit of evaporation was used to study the effects of water resources on land resources.

3. Results

3.1. Model Calibration and Verification

After debugging the relevant parameters of the hydrological model, the monthly runoff in the Shuyuan Hydrological Station simulation was compared with the actual natural runoff process, and the relevant simulation index indicators were calculated, as shown in Table 4. The runoff process is shown in Figure 13. The typical groundwater simulation results are shown in Figure 14. The maximum relative error was approximately 40%, and the average relative error was 15%. The results of the basin evaporation simulation are shown in Figure 15. The correlation coefficient was 0.93, and the relative error was 3.9%.

Table 4. Monthly runoff simulation effect indicator of Shuyuan Hydrological Station.

	Annual Average Runoff (10^8 m^3)		Relative Error (%)	Nash Coefficient	Correlation Coefficient
	Observed	Simulation			
Calibration (1968~1995)	2.34	2.34	0.28	0.62	0.80
Validation (1996~2015)	2.58	2.51	−2.98	0.64	0.85

Note: The simulation time was 1953–2015, excluding the 5-year warm-up period, so the time for calibration and verification was 1968–2015.
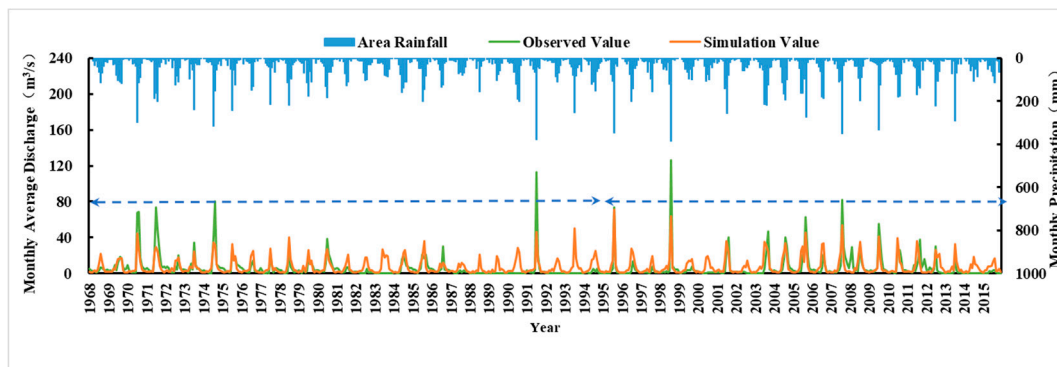
Figure 13. Simulation and observation value comparison of the monthly runoff.
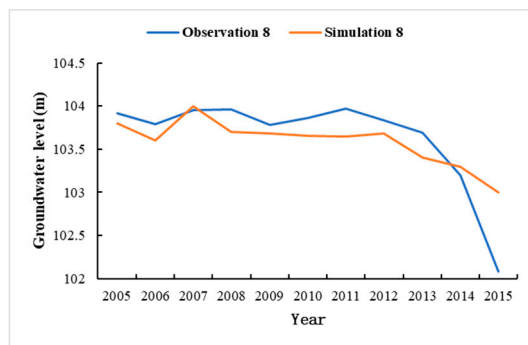
(**a**)
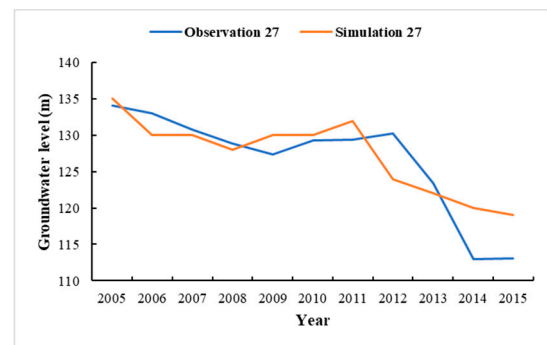
(**b**)

Figure 14. Annual groundwater level simulation and observed values. (**a**): No. 8 groundwater observation well. (**b**): No. 27 groundwater observation well. Note: Groundwater level data were only collected from 2005 to 2015.
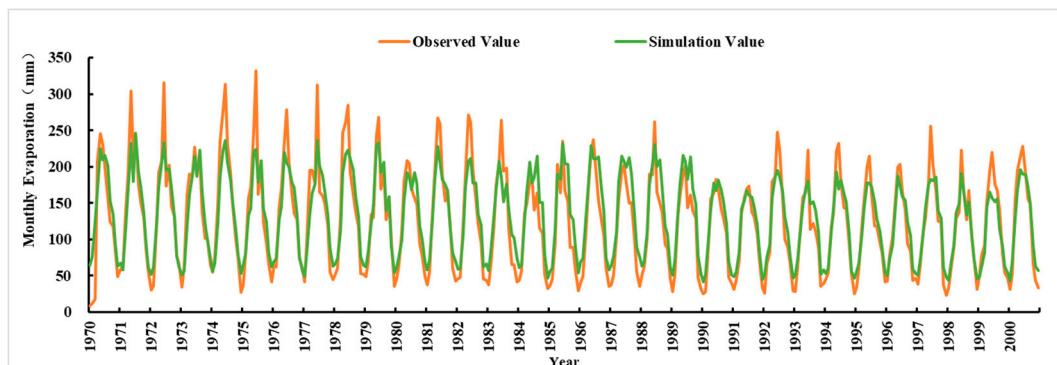
Figure 15. Monthly evaporation simulation and observed values. Note: Evaporation data were only collected from 1970 to 2000.

3.2. The Effect of Land Resources on Water Resources in Sihe River Basin

The spatial distribution of the runoff coefficient is shown in Figure 16. The runoff coefficients of the mountainous areas in the north and south were smaller than those in the central plains. From the 1980s to the present day, the runoff coefficient in mountainous areas has been decreasing, and the runoff coefficient in the plain areas first decreased and then started to increase. From the perspective of land-use types, the runoff coefficient of the grassland areas was greater than that of the cultivated land and woodland areas. From the perspective of topography, basins had the largest runoff coefficients, and hills and plains had similar runoff coefficients. From a time perspective, the runoff coefficients after the year 2000 were higher than they were before the year 2000.
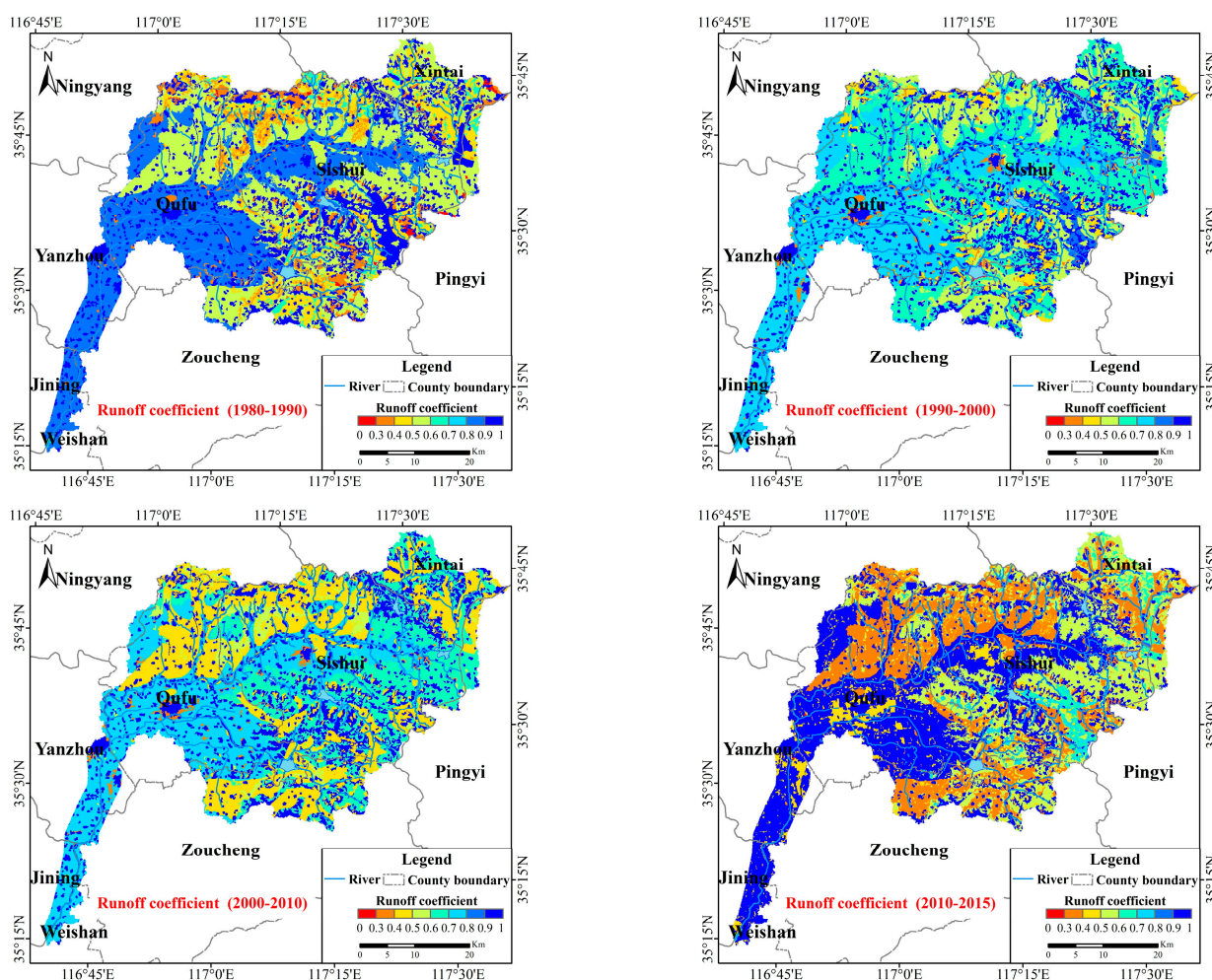
Figure 16. Spatial distribution of runoff coefficient in different periods.

3.3. The Effect of Water Resources on Land Resources in the Sihe River Basin

The spatial distribution of the ratio of NPP to evapotranspiration is shown in Figure 17. The ratios in the north and south were smaller than those in the middle. From the 1980s to the present day, the ratio of the river basin between 2000 and 2010 was higher than in other periods. From the perspective of land-use types, the NPP produced per unit of evaporation in the cultivated land was larger than that in the forest areas, the construction site area was larger than that in the grassland areas, and the cultivated land was approximately 10 times larger than that in the forest land. From the perspective of landform types, basins were larger than plains and hills. From the perspective of time, the average time after 2000 was lower than before 2000.
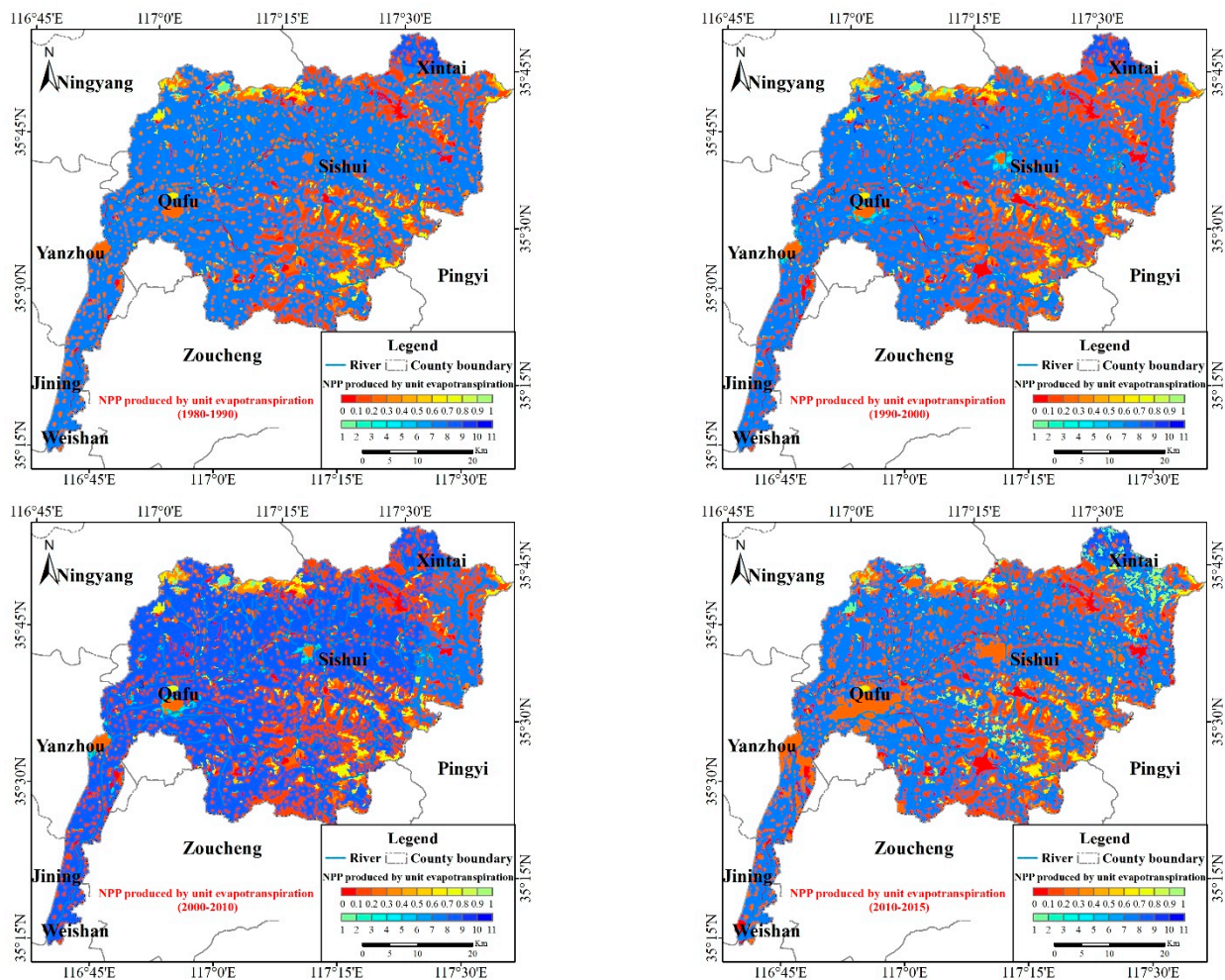
Figure 17. Spatial distribution of NPP produced by unit evaporation in different ages.

4. Discussion

4.1. Model's Performance Evaluation

A complete model evaluation was conducted for the entire period, and the results are shown in Table 4 and Figures 13–15. The dividing time period between the calibration period and the verification period was 1995. The simulated value of the peak surface runoff at the calibration period appeared later than the observed value, and the simulated peak value during the verification period was close to the observed value, which resulted in the correlation coefficient during the calibration period being smaller than that during the verification period. Under the same rainfall conditions, the runoff during the verification period was greater than it was during the calibration period. This resulted in a relative error during the verification period that was greater than it was during the calibration period. Circa 1990, the distribution of rainfall during the flood season (between June and September) changed. Before the 1990s, the multi-year average percentages of June, July, August and September of the total rainfall during the flood season were 18.2%, 42.5%, 24.7% and 14.5%, respectively. However, after the 1990s, the multi-year average percentages of June, July, August and September of the total rainfall during the flood season were 16.6%, 37.6%, 32.4% and 13.3%, respectively. The change in the distribution of rainfall during the flood season is one of the reasons for the change in the relationship between the rainfall and runoff [19,20]. In addition, after the 1990s, the rapid development of urbanization and the intensification of human activities led to huge changes in the underlying surface. From the 1980s to the present day, cultivated land in the river basin has decreased by 3.2%, forest land has decreased by 0.7% and grassland has decreased by 2.7%, whilst

water bodies have increased by 1.4%, and residential/industrial land has increased by 5%. This is another important reason for the changes in the relationship between rainfall and runoff [21]. Compared with previous studies, the simulation results for the total runoff in this study were better, but the correlation coefficient and Nash coefficient were lower [22]. Therefore, there is room for further improvement in this model.

The refined distributed hydrological model devised in this study has three advantages. First, it was classified according to the data reprocessing. Second, the hydrological cycle models of the different underlying surface types were compiled, which can be used to study the water cycle processes of different underlying surface types. Third, each grid unit had its own vertical water cycle process, which can be used to study the spatial law of the water cycle.

In this study, the coupling between the simulations of the surface and underground water processes were considered while compiling this model. Absorbing the advantage of the WEP model and the MOFLOW model, a new set of models were rewritten to make the model simulation elements more comprehensive, the simulation method more complete and the simulation results more reasonable.

4.2. The Impact of Land Resources on Water Resources

Due to the combined effects of human activities and the environment, the types and functions of land use are constantly changing [23]. These changes also profoundly affect the water cycle processes in river basins [24]. This study simulated and calculated the spatial distribution of runoff coefficients. The results showed that the runoff coefficient was as follows: residential/industrial land > grassland > forest land > cultivated land. This is because the soil infiltration capacity of cultivated land is greater than that of other land-use types [25]. From the perspective of vegetation coverage and the leaf area index, residential/industrial land was the smallest, while forest land, grassland and cultivated land showed seasonal changes, which led to different effects on evapotranspiration and rainfall interception [26]. The runoff coefficient of the basin was greater than that of the hills and plains, mainly because most of the residential/industrial land and water bodies are distributed in the basin, and the direct runoff method is dominant in residential/industrial land [27]. Human activities and climate change are leading to extreme rainfall and are affecting runoff coefficients [28,29]. Science in the 20th century and the continuous development of farming technology (e.g., subsoiling, etc.) has improved the landforms of farmland areas. Furthermore, the infiltration capacity and the water storage capacity of the soil have also been improved, resulting in a reduction in the runoff coefficient [18]. Forest and grassland areas have a strong water-holding capacity; however, due to rainwater being intercepted by leaves and litter, the precipitation is mostly returned to the atmosphere in the form of evaporation [30]. In the process of runoff generation, the main runoff method on cultivated land is infiltration excess runoff, while in forest and grassland areas it is saturation excess runoff. Moreover, evapotranspiration in forest and grassland areas is higher than it is on cultivated land, which makes the runoff coefficient of cultivated land higher than that of the forest and grassland areas.

4.3. The Impact of Water Resources on Land Resources

NPP refers to the total amount of organic carbon that has been fixed by vegetation through photosynthesis (per unit area and unit time), with its own respiration consumption for plant growth deducted [31]. Different types of land grow different types of vegetation, which leads to different levels of photosynthesis, which, in turn, affects the production efficiency of the land [32]. The land-use pattern is the main factor that affects NPP [33], and water is the main factor that affects photosynthesis [34]. NPP reflects the ability of plants to accumulate organic matter during growth [35], but it does not reflect the efficiency of water resources. In this study, the ratio of NPP to evapotranspiration was used to study the impact of water resources on land resources. The NPP per unit area was as follows: forest > cultivated land > residential/industrial land > grassland. However, the

evapotranspiration per unit area was as follows: forest > grassland > residential/industrial land > cultivated. The results showed that the highest NPP per unit of evapotranspiration was in cultivated land, which was approximately 10 times that of forest land. This showed that, from the perspective of the impact of water resources on the productivity of land resources, the efficiency of cultivated land was the highest. Imhoff et al.'s research also showed that the occupation of cultivated land in the process of urbanization leads to a decrease in NPP [36]. Weinhold's research in the Amazon region showed that land productivity declines when forest land is converted to cultivated land [37]. Similarly, scholars have studied the water use efficiency of ecosystems through the ratio of the photosynthetic CO_2 assimilation rate to the ET rate [38]; the ratio of net ecosystem carbon exchange to the ET (NEE/ET) [39]; and the ratio of the gross primary productivity to the ET (GPP/ET) [40]. The results showed that forest land is larger than grassland, which is consistent with the research results of this study.

5. Conclusions

In this study, we attempted to couple surface water and groundwater cycle simulations and to write a hydrological model in Python. The monthly runoff and annual groundwater level tests showed that the model was effective for surface water simulations, but that the groundwater station simulation needs to be further improved. For this paper, we studied the spatial distribution of the surface runoff coefficient and the mutual influence of water and land resources.

The results showed that forest land had an obvious effect on runoff regulation. The main reason for this was the influence of the soil water content and evapotranspiration. Among the topographical factors, slopes had a greater influence on runoff generation. The NPP produced by the average unit of evapotranspiration in cultivated land and basins was the largest. This showed that units' water resources showed the greatest efficiency in cultivated land. Hills showed the least water efficiency, mainly because they are not suitable for production and planting due to the influence of the terrain.

In the process of compiling the hydrological model used in this study, the underground simulation did not consider the exchange relationship between the river channel and the soil vadose zone, nor did it consider the influence of groundwater recharging and evaporation. In addition, the influence of vegetation growth and root changes on water absorption was not considered in the process of the soil water cycle simulation. In the future, to improve the model, it will be necessary to further strengthen the research into these physical mechanisms through field experiments and indoor simulations.

Author Contributions: J.W. drafted the manuscript; T.Q. and X.L. designed the project and provided overall guidance; H.N., Z.L., C.L., X.Z. and J.F. provided the simulation method; J.W. and T.Q. finalized the manuscript; Y.N., L.M. and Q.Z. collected the data. All authors have read and agreed to the published version of the manuscript.

Data Availability Statement: The datasets used and/or analysed during the current study available from the corresponding author on reasonable request.

Conflicts of Interest: The authors declare no conflict of interest.

References

1. Wang, X.; Zhang, J.; Shahid, S. Forecasting Industrial Water Demand in Huaihe River Basin Due to Environmental Changes. *Mitig. Adapt. Strateg. Glob. Chang.* **2017**, *23*, 469–483. [CrossRef]
2. Liu, X.; Cai, Z.; Xu, Y.; Zheng, H.; Wang, K.; Zhang, F. Suitability Evaluation of Cultivated Land Reserved Resources in Arid Areas Based on Regional Water Balance. *Water Resour. Manag.* **2022**, *36*, 1463–1479. [CrossRef]
3. Geng, Q.; Liu, H.; He, X.; Tian, Z. Integrating Blue and Green Water to Identify Matching Characteristics of Agricultural Water and Land Resources in China. *Water* **2022**, *14*, 685. [CrossRef]
4. Wu, P.; Christidis, N.; Stott, P. Anthropogenic Impact on Earth's Hydrological Cycle. *Nat. Clim. Chang.* **2013**, *3*, 807–810. [CrossRef]
5. Matusick, G.; Ruthrof, K.X.; Kala, J.; Brouwers, N.C.; Breshears, D.D.; Hardy, G.E.S.J. Chronic Historical Drought Legacy Exacerbates Tree Mortality and Crown Dieback during Acute Heatwave-Compounded Drought. *Environ. Res. Lett.* **2018**, *13*, 095002. [CrossRef]
6. Zeppel, M.J.B.; Wilks, J.V.; Lewis, J.D. Impacts of Extreme Precipitation and Seasonal Changes in Precipitation on Plants. *Biogeosciences* **2014**, *11*, 3083–3093. [CrossRef]
7. Bayat, M.; Alizadeh, H.; Mojaradi, B. SWAT_DA: Sequential Multivariate Data Assimilation-Oriented Modification of SWAT. *Water Resour. Res.* **2022**, *58*, e2022WR032397. [CrossRef]
8. Zhang, L.; Lei, H.; Shen, H.; Cong, Z.; Yang, D.; Liu, T. Evaluating the Representation of Vegetation Phenology in the Community Land Model 4.5 in a Temperate Grassland. *J. Geophys. Res. Biogeosci.* **2019**, *124*, 187–210. [CrossRef]
9. Yang, T.; Šimůnek, J.; Mo, M.; Mccullough-Sanden, B.; Shahrokhnia, H.; Cherchian, S.; Wu, L. Assessing Salinity Leaching Efficiency in Three Soils by the HYDRUS-1D and -2D Simulations. *Soil Tillage Res.* **2019**, *194*, 104342. [CrossRef]
10. Jeppesen, J.; Christensen, S.; Ladekarl, U.L. Modelling the Historical Water Cycle of the Copenhagen Area 1850–2003. *J. Hydrol.* **2011**, *404*, 117–129. [CrossRef]
11. Dash, S.S.; Sahoo, B.; Raghuwanshi, N.S. How Reliable Are the Evapotranspiration Estimates by Soil and Water Assessment Tool (SWAT) and Variable Infiltration Capacity (VIC) Models for Catchment-Scale Drought Assessment and Irrigation Planning? *J. Hydrol.* **2021**, *592*, 125838. [CrossRef]
12. Papadimos, D.; Demertzi, K.; Papamichail, D. Assessing Lake Response to Extreme Climate Change Using the Coupled MIKE SHE/MIKE 11 Model: Case Study of Lake Zazari in Greece. *Water* **2022**, *14*, 921. [CrossRef]
13. Jia, Y.; Ni, G.; Kawahara, Y.; Suetsugi, T. Development of WEP Model and Its Application to an Urban Watershed. *Hydrol. Process.* **2001**, *15*, 2175–2194. [CrossRef]
14. Penman, H.L. Natural Evaporation from Open Water, Hare Soil and Grass. *Proc. R. Soc. Lond. Ser. A Math. Phys. Sci.* **1948**, *193*, 120–145. [CrossRef]
15. Noilhan, J.; Planton, S. A Simple Parameterization of Land Surface Processes for Meteorological Models. *Mon. Weather Rev.* **1989**, *117*, 536–549. [CrossRef]
16. Jia, Y.; Tamai, N. Modeling Infiltration into a Multi-Layered Soil during an Unsteady Rain. *J. Hydrosci. Hydraul. Eng.* **1998**, *41*, 31–36. [CrossRef]
17. Harbaugh, A.W. *MODFLOW-2005, The US Geological Survey Modular Ground-Water Model: The Ground-Water Flow Process*; v.1.12.00; US Department of the Interior: Washington, DC, USA; US Geological Survey: Reston, VA, USA, 2005.
18. Pikul, J.L.; Aase, J.K. Water Infiltration and Storage Affected by Subsoiling and Subsequent Tillage. *Soil Sci. Soc. Am. J.* **2003**, *67*, 859. [CrossRef]
19. Kwon, H.H.; Brown, C.; Xu, K.; Lall, U. Seasonal and Annual Maximum Streamflow Forecasting Using Climate Information: Application to the Three Gorges Dam in the Yangtze River Basin, China. *Hydrol. Sci. J.* **2009**, *54*, 582–595. [CrossRef]
20. Kim, S.; Kim, B.S.; Jun, H.; Kim, H.S. Assessment of Future Water Resources and Water Scarcity Considering the Factors of Climate Change and Social–Environmental Change in Han River Basin, Korea. *Stoch. Environ. Res. Risk Assess.* **2014**, *28*, 1999–2014. [CrossRef]
21. Zhou, Z.; Jia, Y.; Qiu, Y.; Liu, J.; Wang, H.; Xu, C.Y.; Li, J.; Liu, L. Simulation of Dualistic Hydrological Processes Affected by Intensive Human Activities Based on Distributed Hydrological Model. *J. Water Resour. Plan. Manag.* **2018**, *144*, 04018077. [CrossRef]
22. Wang, J.; Wang, K.; Qin, T.; Lv, Z.; Li, X.; Nie, H.; Liu, F.; He, S. Influence of Subsoiling on the Effective Precipitation of Farmland Based on a Distributed Hydrological Model. *Water* **2020**, *12*, 1912. [CrossRef]
23. Vadrevu, K.; Heinimann, A.; Gutman, G.; Justice, C. Remote Sensing of Land Use/Cover Changes in South and Southeast Asian Countries. *Int. J. Digit. Earth* **2019**, *12*, 1099–1102. [CrossRef]
24. Dong, G.; Yang, Z.; Yu, Y. Research progress on effects of variations of underlying surface on runoff yield and concentration in the river basin. *South North Water Transf. Water Sci. Technol.* **2013**, *11*, 111–117, 126. (In Chinese)
25. Li, X.Y.; Contreras, S.; Solé-Benet, A.; Cantón, Y.; Domingo, F.; Lázaro, R.; Lin, H.; Van Wesemael, B.; Puigdefábregas, J. Controls of Infiltration-Runoff Processes in Mediterranean Karst Rangelands in SE Spain. *CATENA* **2011**, *86*, 98–109. [CrossRef]
26. Gao, Y.; Chen, F.; Jiang, Y. Evaluation of a Convection-Permitting Modeling of Precipitation over the Tibetan Plateau and Its Influences on the Simulation of Snow-Cover Fraction. *J. Hydrometeorol.* **2020**, *21*, 1531–1548. [CrossRef]
27. Nie, W.; Yuan, Y.; Kepner, W.; Nash, M.S.; Jackson, M.; Erickson, C. Assessing Impacts of Landuse and Landcover Changes on Hydrology for the Upper San Pedro Watershed. *J. Hydrol.* **2011**, *407*, 105–114. [CrossRef]
28. Tomkins, K.M. Uncertainty in Streamflow Rating Curves: Methods, Controls and Consequences. *Hydrol. Process.* **2014**, *28*, 464–481. [CrossRef]

29. Rose, S.; Peters, N.E. Effects of Urbanization on Streamflow in the Atlanta Area (Georgia, USA): A Comparative Hydrological Approach. *Hydrol. Process.* **2001**, *15*, 1441–1457. [CrossRef]

30. Hughes, D.A. A Review of 40 Years of Hydrological Science and Practice in Southern Africa Using the Pitman Rainfall-Runoff Model. *J. Hydrol.* **2013**, *501*, 111–124. [CrossRef]

31. Liu, J.; Chen, J.M.; Cihlar, J.; Chen, W. Net Primary Productivity Distribution in the BOREAS Region from a Process Model Using Satellite and Surface Data. *J. Geophys. Res. Atmos.* **1999**, *104*, 27735–27754. [CrossRef]

32. Wang, J.; Li, A.; Jin, H. A review on research advances in estimation models for Net PrimaryProduction of vegetation in wetlands production of vegetation in wetlands. *Wetl. Sci.* **2015**, *13*, 636–644. (In Chinese)

33. Gao, Z.Q.; Liu, J.Y.; Cao, M.K.; Li, K.R.; Tao, B. Impacts of Land Use and Climate Change on Regional Net Primary Productivity. *Acta Geogr. Sin.* **2004**, *59*, 581–591.

34. Yue, D.; Zhou, Y.; Guo, J.; Chao, Z.; Guo, X. Relationship between Net Primary Productivity and Soil Water Content in the Shule River Basin. *CATENA* **2022**, *208*, 105770. [CrossRef]

35. Zhang, M.; Chen, S.; Jiang, H.; Peng, C.; Zhang, J.; Zhou, G. The Impact of Intensive Management on Net Ecosystem Productivity and Net Primary Productivity of a Lei Bamboo Forest. *Ecol. Model.* **2020**, *435*, 109248. [CrossRef]

36. Imhoff, M.L.; Tucker, C.J.; Lawrence, W.T.; Stutzer, D.C. The Use of Multisource Satellite and Geospatial Data to Study the Effect of Urbanization on Primary Productivity in the United States. *IEEE Trans. Geosci. Remote Sens.* **2000**, *38*, 2549–2556. [CrossRef]

37. Weinhold, D. Estimating the Loss of Agricultural Productivity in the Amazon. *Ecol. Econ.* **1999**, *31*, 63–76. [CrossRef]

38. Group, S.P.; Systems, F. Comparison of Ecosystem Water-Use Efficiency among Douglas-Fir Forest, Aspen Forest and Grassland Using Eddy Covariance and Carbon Isotope Techniques. *Glob. Chang. Biol.* **2006**, *12*, 294–310. [CrossRef]

39. Hu, Z.; Yu, G.; Wang, Q.; Zhao, F. Ecosystem level water use efficiency: A review. *Acta Ecol. Sin.* **2009**, *29*, 1498–1507. (In Chinese)

40. Law, B.E.; Falge, E.; Gu, L.; Baldocchi, D.D.; Bakwin, P.; Berbigier, P.; Davis, K.; Dolman, A.J.; Falk, M.; Fuentes, J.D.; et al. Environmental Controls over Carbon Dioxide and Water Vapor Exchange of Terrestrial Vegetation. *Agric. For. Meteorol.* **2002**, *113*, 97–120. [CrossRef]